IEEE Access
Multidisciplinary ⋮ Rapid Review ⋮ Open Access Journal

Received May 9, 2022, accepted May 27, 2022, date of publication June 3, 2022, date of current version June 13, 2022.

Digital Object Identifier 10.1109/ACCESS.2022.3179973

A Novel Pre-Storm Island Formation Framework to Improve Distribution System Resilience Considering Tree-Caused Failures

MAHDI BAHRAMI[1], MEHDI VAKILIAN[1], (Senior Member, IEEE), HOSSEIN FARZIN[2], AND MATTI LEHTONEN[3]

[1]Department of Electrical Engineering, Sharif University of Technology, Tehran 11365-11155, Iran
[2]Faculty of Engineering, Shahid Chamran University of Ahvaz, Ahvaz 61357-43337, Iran
[3]Department of Electrical Engineering and Automation, Aalto University, 00076 Espoo, Finland

Corresponding author: Matti Lehtonen (matti.lehtonen@aalto.fi)

This work was supported in part by the Iran National Science Foundation (INSF) under Grant 98009638.

ABSTRACT This paper presents a new framework for island formation prior to windstorms, which considers tree-caused failures of distribution networks. In the proposed framework, both direct and indirect effects of windstorms on distribution lines are quantified. Thus, a novel discrete Markov chain model is proposed for representing the failure modes of trees in each time interval of windstorm duration. This model categorizes ''healthy'', ''uprooted'', ''stem breakage'', and ''branch breakage'' states of a tree. In addition, a new line-tree interaction model is presented for calculating tree-caused failure probability of overhead lines. The results of the proposed Markov model are taken as inputs by the developed line-tree interaction model. In these models, the different characteristics of windstorms are taken into account. Tree vulnerability to windstorms is characterized by different factors such as their species, height, and critical wind speeds. Windstorm duration is sectionalized into multiple time intervals, and the proposed models are applied to trees and distribution system components in each interval. Moreover, the interdependency between the intervals is captured by the Markov model. The results of the models are used by an optimization model, thereby dividing a distribution system into multiple islands before storm onset. Subsequently, the framework is extended as a two-stage stochastic optimization problem to address the uncertainties of loads. In addition, this framework considers the allocation of mobile emergency resources. The proposed models are implemented on the IEEE 33- and 123-bus test systems, as well as a practical distribution feeder, and their effectiveness is demonstrated through several case studies.

INDEX TERMS Discrete Markov chain, distributed energy resources (DERs), distribution system resilience, microgrids, mobile emergency resource (MER), tree failures, windstorms.

NOMENCLATURE

A. INDICES AND SETS

s	Index of scenario.
ω	Index for stage number of stochastic programming problem.
t, τ	Index of time and storm time interval.
T, Ω_T	Index and set of trees.
i, Ω_N	Index and set of nodes.
j, Ω_B	Index and set of distribution branches.
g, Ω_{DER}	Index and set of DERs.
cl, Ω_{CL}	Index and set of critical loads.
m, Ω_{MER}	Index and set of mobile emergency resources, respectively.

B. PARAMETERS AND CONSTANTS

P^f	Failure probability.
$v_{g,n}^{\max}$	Maximum wind speed at time interval n of storm.
CW_{Up}, CW_{SB}	The critical wind speeds at which a tree is uprooted and trunk snapped, respectively.
$\Gamma(n)$	The stochastic transitional probability matrix of a tree in time interval n.
$\tilde{\pi}(n)$	Vector of state probability for a tree in time interval n of windstorm.

The associate editor coordinating the review of this manuscript and approving it for publication was Fabio Mottola.

h_T, h_T^e	The tree height and the effective tree height, respectively.
$h_T^{e,im}$	Image of the effective tree height on the ground.
h_L	The height of distribution lines above the ground.
ϑ_T	A binary parameter indicating whether the stem or branches of tree T can fall on the adjacent line or not, with regard to wind direction.
$\Delta\varphi$	The fluctuation parameter in the wind direction.
ζ	A fraction of tree stem that is broken by storm and falls on the ground.
d	The horizontal distance between a tree and its adjacent distribution line.
r_{ij}, x_{ij}	Resistance and reactance of branch ij.
δ	A binary parameter indicating a distribution component is in a healthy condition or not.
$P_{i,t}^D$, $Q_{i,t}^D$	Active and reactive demand at bus i, at time t.
Tr	Vulnerability threshold.
χ_1, χ_2	$\text{Min}(d_1, d_2)$ and $\text{Max}(d_1, d_2)$, respectively.

C. VARIABLES AND FUNCTIONS

α	A binary variable indicating if a distribution component is energized or not. (1/0)
$\psi_{m,i}$	A binary variable specifying if mobile emergency resource m is allocated to node i before storm arrival or not. (1/0)
$P_{i,t}^{sh}$, $Q_{i,t}^{sh}$	Active and reactive amount of load shedding at node i, at time t
$P_{ij,t}$, $Q_{ij,t}$	Active and reactive power flow in distribution branch ij, at time t.
$P_{g,t}^G$, $Q_{g,t}^G$	Active and reactive power generation by DER g, at time t.
$V_{i,t}$	Voltage magnitude of node i, at time t

D. SYMBOLS AND ACRONYMS

f	Symbol for failure.
l, p	Symbols for line and pole, respectively.
di, ind	Symbols for direct and indirect, respectively.
Up, SB	Symbols for uprooted and stem breakage.
He, BB	Symbols for healthy and branch breakage, respectively.
Min, max	Symbols for minimum and maximum, respectively.
SE	Priority-weighted supplied energy.

I. INTRODUCTION

Weather-related incidents can make adverse impacts on power grids [1]. In this context, resilience-oriented measures should be taken by system operators. In particular, operation-oriented proactive measures play a critical role in improving distribution system resilience [2]. In order to implement these measures, it is necessary to anticipate outages in distribution systems (DSs) [3], [4].

Severe windstorms have catastrophic impacts on power system components. In this context, development of the models that can predict component outages prior to the storms is a crucial task for power grid utilities [5]. Indeed, outage prediction can significantly impact the storm-related efforts of electric utilities [6]. Based on the results of the outage prediction, they can plan their emergency storm response. For example, the utilities can estimate the amount of repair resources required to repair the possible damages. In the case of windstorms, trees are the dominant cause of DS component failures [7], [8]. In this regard, trees must be incorporated into the storm-related studies of DSs. However, modeling the tree-caused failures is a difficult task. The difficulty lies in the stochastic behavior of trees during storms [9].

In the literature, several methods have been developed for modeling the tree failures during windstorms, which can be divided into three groups: 1-explanatory, 2-mechanistic, and 3-statistical models [10]. In the explanatory models, the causal relationships between different factors, such as species and dimensions, are investigated. These models are suitable for the conditions in which there are not sufficient historical data [10]. In the mechanical wind-risk models, wind loading on trees is analyzed, and accordingly the failure probability of trees during windstorms is calculated [11], [12]. The mechanical models require some detailed data for each tree, such as tree mass [13]. Nonetheless, it is very difficult to collect such detailed data for all trees. Statistical modeling techniques aim at predicting tree damage probability using the machine learning methods [14], [15]. To do so, they need tree-related data such as tree locations and heights for different windstorms and locations. Based on the above discussion, it can also be confirmed that the referred papers only focus on tree damage modeling, and do not investigate the effects of tree failures on power lines.

There are some studies that have focused on power outage prediction during normal weather condition [16]–[18], which are not applicable under windstorms. To address this concern, a variety of methods have been proposed in the past-published studies to predict the storm-caused outages, which can be broadly classified into two main categories: 1- fragility-based approaches 2- statistical models [19]. In the first category, [19] estimates power outages during disasters based on fragility curves. In the second category, [20] develops an outage-forecasting model based on the random forest method. Likewise, a statistical model in [21] is presented for power outage prediction during typhoons. In addition to the power grid data, this model considers meteorological and geographical factors. However, there are few papers that quantify tree-induced failures of DS components during windstorms. In this group, the authors in [22] propose a method in which the effects of windstorms on DSs are evaluated through

sequential Monte Carlo simulation method. In this paper, a linear relationship between the failure rate of components in normal and windstorm conditions is established. Likewise, [5] proposes a framework for assessing transmission system availability in the case of extreme weather events. In this study, the effect of tree falling on power components is considered through failure rates of components. The authors in [23] proposed an outage prediction model for DSs during storms. In this model, machine learning method is used for predicting power outages. Reference [8] uses a statistical model to predict the locations and number of hurricane-caused outages for a utility located in the coastal Gulf of Mexico areas. In this model, some tree-related variables such as tree species are added to the model. Nevertheless, trees have different failure modes whose effects on distribution branches are not identical. Hence, it is necessary to distinguish between them. Moreover, possible impacts of damaged trees on power lines have not been properly analyzed in the existing literature.

Microgrid formation against extreme events has been recognized as an effective strategy for reducing the impacts of extreme events on DSs [24]. In this regard, several studies in the literature investigated the role of microgrids in serving critical loads in the event of natural disasters. They can be classified into two categories of post-disaster and pre-disaster microgrid-forming studies. The studies in the first group construct microgrids in the aftermath of disasters. For example, a distributed secondary control strategy is developed in [25], which forms microgrids with dynamic borders after natural disasters. The authors in [26] propose an integrated optimization model that dynamically forms microgrids after extreme events. In this study, the optimal dispatch of repair crews is determined as well. In [27], an algorithm for the construction of network microgrids after a natural disaster is developed. In this algorithm, Petri nets are utilized for recognizing the status of healthy components. In contrast, a few papers in the second category have focused on constructing microgrids before the arrival of disasters. For example, the authors in [28] propose a heuristic method for solving the two-stage optimization problem. In the first stage, the optimal locations of distributed generators (DGs) are determined prior to disaster onset, and the second stage constructs microgrids in the aftermath of the disasters. In [29] and [30], a proactive microgrid formation against windstorms and floods is presented. Nevertheless, to the best of authors' knowledge, none of these studies covers the task of modeling the tree-caused failures. However, there are some studies that propose hardening-oriented measures for improving DS resilience against windstorms. For example, an optimal hardening strategy is presented in [31] that enhances the resilience of a DS against storms. Three resilience-enhancement strategies are considered, including the vegetation management. Nonetheless, operational and hardening measures are two complementary actions to make a DS more resilient against windstorms. Consequently, utility companies should implement these two resilient-oriented measures.

Motivated by the aforementioned challenges, this paper proposes a novel framework that not only models the three main failure modes of trees during windstorms, but also evaluates the effects of each tree failure mode on its adjacent distribution lines. In this framework, the duration of a windstorm is divided into multiple time intervals. In addition, both direct (wind-induced damages) and indirect (tree-caused damages) effects of windstorms on overhead structures are addressed. Since the stochastic behavior of a tree during storms can be modeled by analyzing Markov models in series, a new discrete Markov chain model is developed to categorize the possible states of an individual tree during each time interval of windstorm duration. In this context, 'healthy', 'uprooted', 'stem breakage', and 'branch breakage' are recognized for a tree by the Markov model. Transition probabilities of this Markov model are computed based on the characteristics of trees and windstorms in each time interval. Subsequently, a novel line-tree interaction model is presented, whereby the tree-caused failure probability of overhead distribution lines is calculated. To this end, the probability of residing in each state of the Markov model is imported as inputs to the line-tree interaction model. Subsequently, the line-tree interaction model is employed to quantify the impact of each failure mode of trees on their adjacent overhead lines. In the next step, the results of the line-tree interaction models are utilized as inputs to the optimization problem, thereby identifying storm-vulnerable lines. Finally, the optimization problem for constructing islands prior to windstorms is expressed in the form of a mixed-integer linear programming (MILP) model. The objective is to maximize the priority-weighted supplied energy to critical loads, while minimizing the vulnerability of energized lines during windstorms. In order to address the uncertainty associated with load demands, the proposed deterministic framework is extended, and a two-stage stochastic framework is proposed. In this stochastic framework, the optimal allocation of mobile emergency resources (MERs) is incorporated. On these bases, the main contributions of this paper can be listed as follows:

- A new Markov model is proposed for identifying the states in which a tree can reside in each time interval of the storm duration, and the associated transition probabilities are calculated based on the tree and windstorm characteristics. The obtained transition probabilities are subsequently used to calculate the probability of residing in each tree state during a storm.
- A novel line-tree interaction model is proposed for calculating tree-induced failure probability of overhead lines for each failure mode of a tree during windstorms.
- The vulnerable branches to an approaching storm are identified using the proposed framework, and an optimization model is presented that constructs islands prior to the storm.
- The proposed deterministic framework is extended to consider load demand uncertainties and pre-storm allocation of MERs.

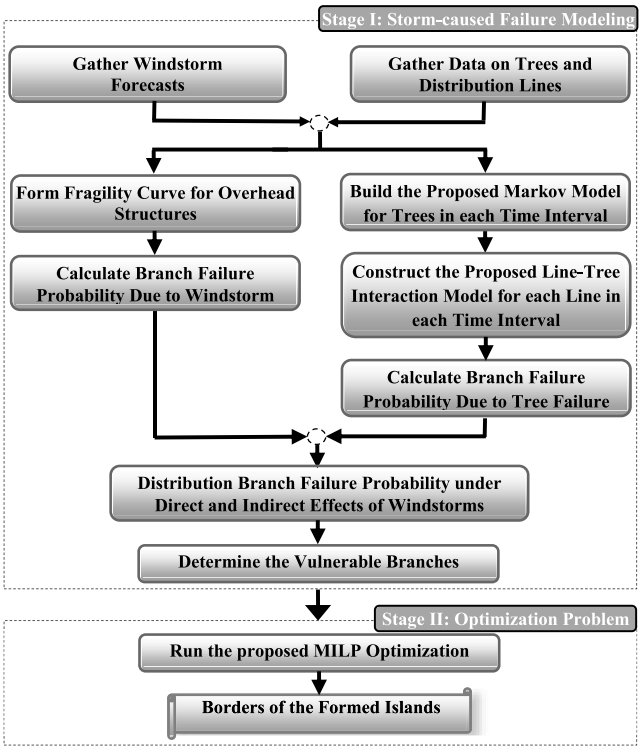

FIGURE 1. General structure of the proposed framework.

The rest of this paper is organized as follows. Section II presents the general overview of the proposed deterministic framework. The details of the proposed Markov and line-tree interaction models are presented in Section III. Section IV formulates the proposed island formation framework in form of a MILP problem. In Section V, the two-stage stochastic framework and its formulation are introduced. Section VI presents and discusses the simulation results on three test systems and finally, summary conclusions are provided in Section VII.

II. PROPOSED FRAMEWORK

In this section, the general structure of the proposed framework is described. Subsequently, an illustrative example is shown so as to implement the framework on a simple distribution network.

A. GENERAL DESCRIPTION OF THE PROPOSED FRAMEWORK

The overall structure of proposed method is depicted in Fig. 1. The proposed framework consists of two stages. In the first stage, all of the distribution lines vulnerable to windstorms are identified. To do so, the proposed Markov and line-tree interaction models are utilized. In the second stage, the proposed framework is implemented to form the islands, using the results of the first stage as inputs. The proposed framework is constructed based on the above methodology through the following steps (in each stage):

Stage 1) The first stage calculates the failure probability of overhead distribution lines under direct and indirect effects of windstorms. This stage can be divided into five steps as follows:

Step 1) The information about trees, distribution overhead structures, and windstorm forecasts is collected.

Step 2) The proposed Markov model is constructed for a tree in each time interval of storm duration. In addition, its transition probabilities are calculated based on the characteristics of the tree and the windstorm in that time interval. Based on the results of this model, the failure probability of the tree in each state is computed, for the time interval of interest.

Step 3) Based on the probability values obtained in the previous step, the tree characteristic, and the windstorm features, the proposed line-tree interaction model calculates the tree-caused failure probability of each distribution line (indirect effect) in each time interval of the storm

Step 4) Using the fragility curves, the failure probabilities of the distribution lines and the poles under the direct effect of windstorms are calculated.

Step 5) Based on the obtained results of Steps 3 and 4, the windstorm-vulnerable branches are identified, which are used as the inputs into the second stage.

Stage 2) The second stage optimally constructs islands prior to windstorms, which can be summarized in the following steps:

Step 1) The proposed optimization framework is run.

Step 2) The configurations of the constructed islands are determined.

B. ILLUSTRATIVE EXAMPLE

In this part, the proposed framework is implemented on a sample distribution network, which is shown in Fig. 2. It is assumed that an upcoming windstorm will hit the network, thereby causing three permanent faults along the distribution network.

Using the first-stage results of the proposed framework, three branches 2-3, 6-10, and 14-15 are recognized as vulnerable to the upcoming storm. Two branches 2-3 and 14-15 will be damaged by the fallen trees (indirect effect of storm), while branch 6-10 will be directly damaged by the storm. Afterward, the second stage determines the island borders such that the amount of priority-weighted supplied energy after storm is maximized. At the same time, the vulnerability of the energized branches during the storm is minimized. Thus, two islands are constructed to supply the critical loads. In island 1, three branches are energized. DG 1 supplies

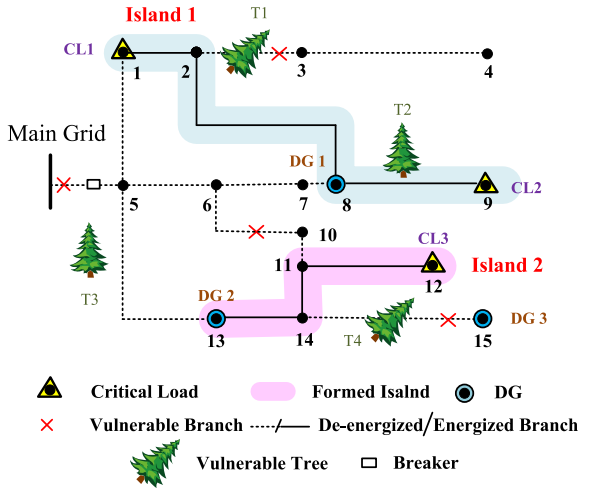

FIGURE 2. Illustrative example of implementing the proposed framework on a sample electricity distribution network.

critical load 1 through branches 1-2 and 2-8. This is because the vulnerability of this path to the upcoming storm is lower than the path involving: 8-7, 7-6, 6-5, and 5-1 branches. In addition, critical load 3 is energized through the island number 2. Moreover, by implementation of this framework, since a tree is located near branch 5-13, this branch will not be energized. This will minimize the vulnerability of the network through energized branches to the upcoming storm.

III. TREE-CAUSED FAILURE MODELING

In this section, the indirect effects of windstorms on distribution lines are modeled. During windstorms, the damages to trees and distribution system components are closely associated with gust wind speeds [32]. Thus, windstorms are characterized by time-based gust speed profile and wind direction in this study. This profile is subsequently divided into some time intervals. In each time interval, the maximum wind speed is used in order to calculate the storm-caused failure probability of the components. On these bases, windstorm dynamic is considered in the proposed framework.

In addition, a tree is modeled considering its general physical features as well as its critical wind speeds. The proposed models are developed for each distribution line and its adjacent trees in each time interval of a storm event. The spatial information about DSs can be accessed through the Geographic Information System (GIS) [33]. Moreover, tree data, such as height, can be derived from LiDAR, tree maps, and satellites [23].

A. DIRECT EFFECT OF WINDSTORMS ON LINES

In order to calculate the failure probability of distribution system components under the direct effects of windstorms, the concept of fragility curves is utilized [34]. To do so, the maximum wind speed during each time interval is mapped onto the fragility curves of overhead components. As a result, the failure probabilities of the components under direct effect of a storm are obtained in each interval.

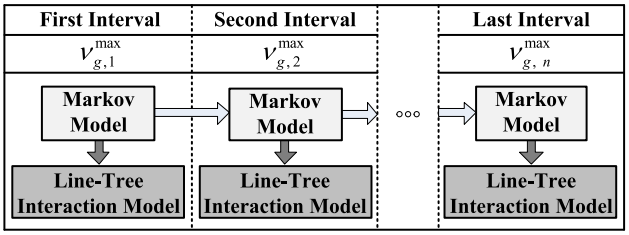

FIGURE 3. Schematic illustration of the dependency between Markov models of a tree during storm time intervals.

B. MODELING INDIRECT EFFECTS OF WINDSTORMS

In this part, a new model is proposed that calculates the tree-induced failure probability of overhead distribution lines during windstorms. This model includes two sub-models. The first one models the random response of an individual tree during windstorms (the Markov model). The second sub-model, however, mathematically computes the tree-induced failure probability of overhead distribution lines for different failure modes of a tree (the line-tree interaction model). These models are constructed in each time interval of storm duration. In addition, the line-tree interaction model is formed in each time interval based on the results of the related Markov model(s) for that interval. In the proposed Markov model, a tree condition at the end of a time interval is considered as the initial state of the tree Markov model in the next time interval. Thus, a chain of Markov models is constructed for modeling the response of a tree during a windstorm. The number of the Markov models used for modeling a tree equals the number of time intervals. This process is schematically illustrated in Fig. 3.

1) PROPOSED DISCRETE MARKOV MODEL

The random behavior of trees during storms can comply with the requirements of Markov models [35]. Therefore, the concept of discrete Markov chain is used in this paper. As mentioned earlier, maximum wind speed is the primary cause of tree failures and power outages during storms. With this in mind, the maximum wind speed in each time interval of storm duration is used to calculate the failure probability of the trees and overhead components. In doing so, the transitional probabilities between different states of the Markov model are a function of maximum wind speed, and they remain constant during a specific time interval. Thus, the stochastic response of a tree in a time interval can be modeled using discrete Markov model. Fig. 4 shows the proposed Markov model for representing the behavior of an individual tree in a time interval of storm duration.

In the proposed Markov model, the states represent different situations of the tree during windstorms. The proposed Markov model addresses four main states for a tree during storms [36], [37]. These states are 'healthy', 'uprooted', 'stem breakage', and 'branch breakage'. In addition, this model represents all of the feasible transitions between the different states of a tree during storms. For example, the uprooted state and the stem breakage state are completely

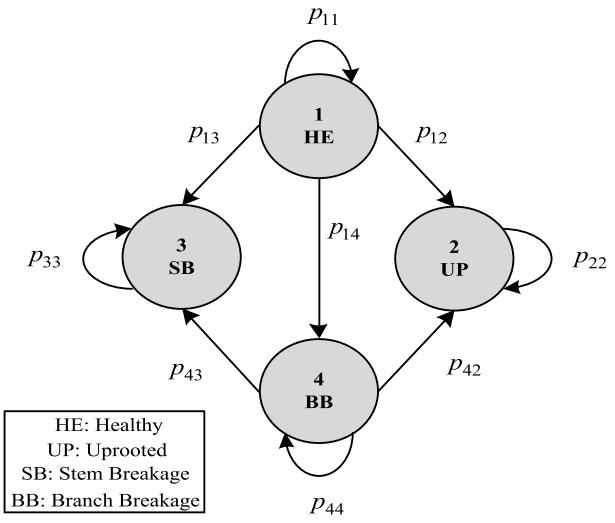

FIGURE 4. Proposed four-state Markov chain for modeling tree response during wind storms in a time interval.

independent. However, in branch breakage state, the trunk of the tree is considered healthy. Thus, a tree which is in the branch breakage state may experience uprooted or stem breakage state in the continuation of a storm event.

If a tree stays healthy in a time interval, the model resides in state 1, with a probability of p_{11}. However, if the tree is uprooted by the windstorm, a transition from state 1 to state 2 occurs with a probability of p_{12}. The windstorm can also cause stem breakage, which makes a transition to state 3 with a probability of p_{13}. Branch breakage is another possible failure mode of the tree, which takes the model to state 4. In this situation, there are three possibilities for the tree. If the wind causes uprooting, the model is taken from state 4 to state 2 with probability p_{42}. In addition, if the tree experiences stem breakage, the model transfers to state 3. Otherwise, it resides in state 4 with probability p_{44}. However, when the model transfers to state 2 (uprooted) or state 3 (stem breakage), it remains in state 2 or state 3 with a probability of 1.

2) MARKOV MODEL TRANSITION PROBABILITIES

The probabilities of the transitions between the Markov states are a function of different parameters, such as wind speed. In this regard, the transition probabilities are determined for each time interval of the windstorm duration, and thus the stochastic transitional probability matrix is constructed for each time interval. On these bases, different transition probabilities of the proposed Markov model are calculated as follows:

$$p_{11} + p_{12} + p_{13} + p_{14} = 1 \tag{1a}$$
$$p_{22} = p_{33} = 1 \tag{1b}$$
$$p_{44} + p_{42} + p_{43} = 1 \tag{1c}$$

Equations (1a)-(1c) account for the probabilities of residing in states 1, 2, and 3 of the proposed Markov model given in Fig. 4. These three equations are derived based on the fact that the summation of the transition probabilities from a Markov state must be equal to unity [35]. Thus, the relationships between the transition probabilities from state 1 and state 4 are respectively expressed by (1a) and (1c). However, if the model enters states 2 or 3, it will remain there. Thus, the value of the corresponding transition probability is equal to unity, which is given by (1b).

The probability of departure from state 1 due to uprooting (p_{12}) and stem breakage (p_{13}) can be calculated using the fragility curves of trees [38]. There are different methods for constructing the fragility curves of trees. In this study, the fragility curves of trees are supplied to the algorithm as inputs, and they can be derived based on the approach presented in [38]. Nonetheless, the proposed framework is general, and when it is difficult to construct such curves for all individual trees, logistic models can be used [39]. These models approximately estimate the windthrow defect (uprooting or stem breakage of trees during high wind speeds) probabilities of the trees. Although when there are a huge number of tree species that have grown in the vicinity of distribution lines, it is difficult to construct the fragility curves for all of them however, it is possible to give the priority of fragility curve construction to the tree species with greater height, shorter distances form lines, and greater majority.

However, p_{12} and p_{13} depend on the critical wind speed for uprooting and the critical wind speed for stem breakage. When the wind speed is lower than both critical speeds, the values of p_{12} and p_{13} are equal to zero [40]. If the wind speed in a time interval is higher than the critical speed and $CW_{sb} < CW_{up}$, the tree is snapped, otherwise it will be uprooted [36]. The other possibility occurs when the wind speed exceeds these two critical wind speeds. In this situation, the tree is either uprooted or snapped. On these bases, p_{12} and p_{13} can be estimated [36]. It should be notified that when a tree is in the standing condition (state 1 or 4), the probabilities of leaving states 1 and 4 due to uprooting or stem breakage are the same. It is due to the fact that the main difference of states 1 and 4 is the broken branches, and the factors that affect the probability of uprooting and stem breakage are not influenced by the broken branches. Therefore, Eqs. (2a) and (2b) are considered.

$$p_{12} = p_{42} \tag{2a}$$
$$p_{13} = p_{43} \tag{2b}$$

Subsequently, using (1) and (2), the stochastic transitional probability matrix, Γ, is constructed for a tree in each time interval of a storm. Finally, the time-dependent probability of being in each tree state after n time intervals is calculated as [35]:

$$\tilde{\pi}(n) = \tilde{\pi}(0) \times \Gamma(1) \times \Gamma(2) \times \ldots \times \Gamma(n) \tag{3}$$

In which, $\tilde{\pi}(0)$ is the initial probability vector of the Markov states.

3) LINE-TREE INTERACTION MODEL

In this subsection, a model is developed for calculating tree-induced failure probability for overhead distribution lines

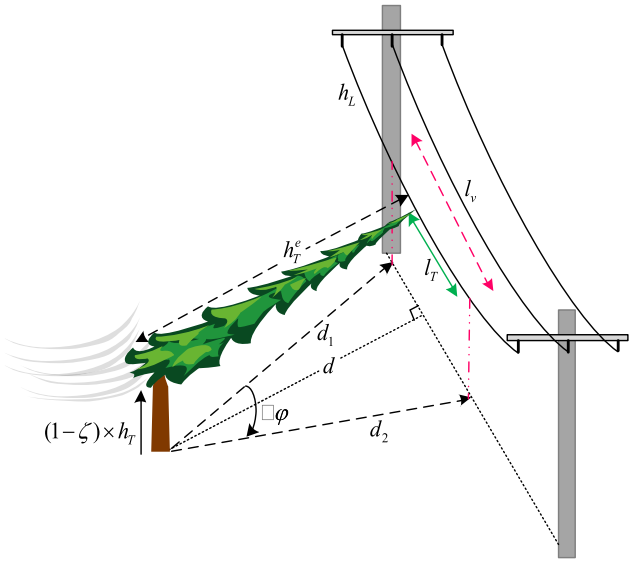

FIGURE 5. Schematic representation of interaction between a damaged tree and its adjacent power line.

during windstorm events. The model is based on the observations made on the tree-caused failures during several windstorms [41]–[43].

The parameters of the line-tree interaction model are illustrated in Fig. 5. In practice, falling trees are in wind direction [36]. In addition, there are a few variations in the direction of windstorm at a region. With this in mind, the wind direction variation is incorporated into the model, which is specified by $\Delta\varphi$ (in degrees). In Fig. 5, d_1 and d_2 indicate the borders of wind direction variation at tree location. In other words, they draw the area borders in which a tree may fall in, if uprooted or broken by wind. The intersection of d_1 and d_2 with the nearest overhead distribution line specifies a fictitious line that a tree may touch, which is represented by l_v. In other words, this fictitious line represents the fraction of a line-section on which tree stem or branches can fall, regarding the direction of windstorms. This line is characterized by wind direction.

Stem breakage occurs at the height of $(1-\zeta)\times h_T$ above the ground. However, in case of uprooting, the whole height of tree is toppled. In order to distinguish between uprooted and stem breakage states, the effective height (h_T^e) is introduced in this model, which stands for the fraction of a tree height that is blown down by windstorms. The effective height for an uprooted tree is represented by $h_{T,up}^e$ and for a snapped tree is represented by $h_{T,sb}^e$, which are defined through the following relations:

$$h_{T,sb}^e = \zeta \times h_T \tag{4a}$$

$$h_{T,up}^e = h_T \tag{4b}$$

$$h_T^{e,im} = \sqrt{(h_T^e)^2 - (h_L - (1-\zeta)h_T)^2} \tag{4c}$$

In (4c), $h_T^{e,im}$ stands for the image of the effective tree height on the ground. If the height of tree is shorter than that of distribution lines, the tree does not threaten its adjacent lines.

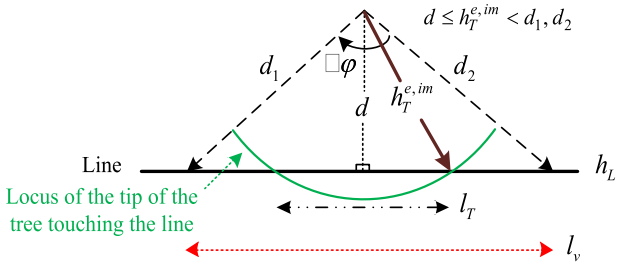

FIGURE 6. Top view of the tree in Fig. 5 for calculation of l_T.

In addition, if $h_T^{e,im}$ is shorter than horizontal distance d, the distribution line is not touched by the fallen trees. On these bases, line l_T is introduced in the model. This line models the fraction of a line that can be touched by tree stem, considering the physical characteristics of the tree located near the tree. Thus, in contrast to l_v, this fictitious line is characterized by both wind direction and effective tree height.

Based on the tree height as well as the location of a tree with respect to its adjacent line, four possibilities for l_T are considered. Based on the parameters given in Fig. 5, the length of l_T for these four possibilities is calculated as follows:

$$l_T = \begin{cases} 0 & h_T^{e,im} < dorh_T < h_L \\ 2 \times \sqrt{(h_T^{e,im})^2 - d^2} & d \le h_T^{e,im} < \chi_1 \& h_L \le h_T \\ \sqrt{(\chi_1)^2 - d^2} + \sqrt{(h_T^{e,im})^2 - d^2} & \chi_1 \le h_T^{e,im} < \chi_2 \& h_L \le h_T \\ l_v & \chi_2 \le h_T^{e,im} \& h_L \le h_T \end{cases} \tag{5}$$

The first possibility occurs when $h_T^{e,im}$ is smaller than the distance between the tree and the distribution line. In this situation, the length of l_T is set to zero, because the fallen tree cannot touch the line. If $h_T^{e,im}$ exceeds the horizontal distance (d), it can touch and damage overhead lines. Therefore, the second, third, and fourth possibilities are considered based on the length of d_1 and d_2. In the fourth possibility, $h_T^{e,im}$ exceeds both d_1 and d_2. In this condition, the fallen tree can touch any point of line between the intersections of the distribution line with d_1 and d_2, and the length of l_T is equal to l_v. Fig. 6 illustrates how the length l_T is calculated, if the second set of inequalities in Eq. (5) are satisfied. In this condition, $h_T^{e,im}$ exceeds d. However, it is smaller than both d_1 and d_2. Thus, based on the Pythagorean theorem, the length of l_T is computed by the second relationship in Eq. (5). Similar figures can be drawn for other relationships in Eq. (5).

In order to compute the tree-caused failure probability for a distribution line, the concept of continuous probability theory is used [44]. Based on this concept, l_v is the continuous sample space, and l_T represents the event of concern. In this case, the concerned event is "fall of the tree on distribution lines". Thus, the failure probability of a line due to uprooting or stem breakage of tree T is determined based on the

following definitions:

$$P_{fa}^{T} = \frac{Length\ of\ concerned\ event}{Length\ of\ sample\ space} = \frac{l_T}{l_v}.\vartheta_T \quad (6a)$$

$$P_{fa,up}^{T} = \frac{l_{T,up}}{l_{v,up}}.\vartheta_T \quad (6b)$$

$$P_{fa,sb}^{T} = \frac{l_{T,sb}}{l_{v,sb}}.\vartheta_T \quad (6c)$$

In (6a), ϑ_T incorporates the effect of wind direction into the tree-induced failure probability of distribution lines. When the wind blows in a direction that a tree does not fall on the distribution lines, the value of ϑ_T is set to 0. Otherwise, it is set to 1. It can be estimated based on forecasted wind speed direction at each location. It should be notified that P_{fa}^{T} is calculated for a line section. In (6b) and (6c), $P_{fa,up}^{T}$ and $P_{fa,sb}^{T}$ account for the failure probability induced by tree T due to uprooting and stem breakage, respectively. Thus, Eqs. (6b) and (6c) are derived from (6a) for uprooted and stem breakage states of tree T, respectively. If tree T threatens more than one distribution line, l_T is computed for each line section.

The uprooted, stem breakage, and branch breakage states might contribute to distribution line failures. Likewise, broken tree branches can result in permanent faults on lines. Furthermore, it is experimentally demonstrated that as the distance between trees and distribution lines increases, the impact of broken tree branches on overhead line failure decreases, which can be modeled by an exponential function [45]. Therefore, the failure probability of a line section, given that some branches of tree T have been broken, is estimated by:

$$P_{fa,bb}^{T} = e^{-(d.\sigma)} \times \kappa \times \vartheta_T \quad (7)$$

In (7), σ is a positive parameter that has correlation with the tree height [45]. In addition, κ stands for the fraction of the falling tree branches that causes permanent faults, and can be estimated using the historical data. As mentioned earlier, each tree state has an occurrence probability that was calculated by (3). Therefore, the tree-induced failure probability of a distribution line due to the three failure modes of an individual tree (i.e. uprooting, stem breakage, and branch breakage) is expressed by:

$$P_{l,T}^{f,ind} = (P_{fa,up}^{T} \times \pi_{up}) + (P_{fa,sb}^{T} \times \pi_{sb}) + (P_{fa,bb}^{T} \times \pi_{bb}) \quad (8)$$

When a distribution line is surrounded by n_T trees, eq. (8) is reformed as follows:

$$P_{l}^{f,ind} = 1 - \prod_{T=1}^{n_T} (1 - P_{l,T}^{f,ind}) \quad (9)$$

Next, the failure probability of a line-section, including both direct and indirect effects of windstorms, is calculated as follows:

$$P_{l}^{f} = P_{l}^{f,di} + P_{l}^{f,ind} - (P_{l}^{f,di}.P_{l}^{f,ind}) \quad (10)$$

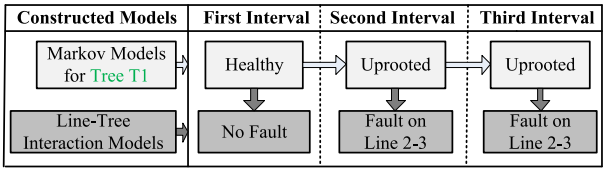

FIGURE 7. The results of the Markov and line-tree interaction models for tree T1 in Fig. 2.

Finally, the failure probability of a distribution branch (with n_p poles and n_l line sections) is calculated as:

$$P_{B}^{f} = P_{Line}^{f} + P_{pole}^{f} - (P_{Line}^{f}.P_{pole}^{f}) \quad (11a)$$

$$P_{pole}^{f} = 1 - \prod_{p=1}^{n_p} (1 - P_{p}^{f}) \quad (11b)$$

$$P_{Line}^{f} = 1 - \prod_{l=1}^{n_l} (1 - P_{l}^{f}) \quad (11c)$$

Equations (11b) and (11c) respectively stand for the failure probability of distribution branch B due to failure of its poles and line-sections.

C. ILLUSTRATIVE EXAMPLE FOR THE PROPOSED MODELS

To clarify the application of the proposed models, they are established for the illustrative example shown in Fig. 2. It is assumed that the duration of the upcoming storm is divided into three time intervals. Therefore, three Markov models are constructed for tree *T1*. The Markov models indicate 4^3 possible combinations for the states of this tree during the storm. Some combinations are associated with tree damage states, in which the tree experiences at least one damage mode. Fig. 7 represents one of the combinations that the tree is uprooted. In this combination, tree *T1* remains in the healthy state during the first interval of the storm. However, the tree is uprooted during the second interval, and it stays in the uprooted state during the continuation of the storm.

Now, three line-tree interaction models are constructed to investigate the possible outcomes of each tree state on its adjacent line, namely line 2-3. For the combination illustrated in Fig. 7, the tree named *T1* is in healthy state in the first interval. Therefore, it does not threaten the line. However, using the line-tree interaction model for the second interval, the probability related to "line 2-3 is damaged due to uprooted tree *T1* ($P_{fa,up}^{T1}$)" is determined. Considering the direction of the storm as well as the height of this tree, the uprooted tree can cause a permanent fault on line 2-3.

Using Eq. (8), the failure probabilities of other damaging states are added to the failure probability of this combination. As a result, the indirect failure probability of line 2-3 due to tree *T1* is obtained ($P_{2-3,T1}^{f,ind}$). In order to calculate Eq. (8), it is required to compute the state probabilities of the tree at the end of each time interval. These probabilities are calculated based on Eq. (3) as follows:

$$\tilde{\pi}(1) = \tilde{\pi}(0) \times \Gamma(1)n = 1 \quad (12a)$$

$$\tilde{\pi}(2) = \tilde{\pi}(0) \times \Gamma(1) \times \Gamma(2)n = 2 \quad (12b)$$

$$\tilde{\pi}(3) = \tilde{\pi}(0) \times \Gamma(1) \times \Gamma(2) \times \Gamma(3) n = 3 \quad (12c)$$

In this example, tree *T1* is in healthy condition prior to the storm arrival. Thus, $\tilde{\pi}(0) = [1\ 0\ 0\ 0]$. In addition, the stochastic transitional probability matrix for this tree in the first time interval is constructed as:

$$\Gamma(1) = \begin{bmatrix} p_{11,1} & p_{12,1} & p_{13,1} & p_{14,1} \\ 0 & p_{22,1} = 1 & 0 & 0 \\ 0 & 0 & p_{33,1} = 1 & 0 \\ 0 & p_{42,1} & p_{43,1} & p_{44,1} \end{bmatrix} n = 1 \quad (13)$$

In a similar manner, this matrix can be constructed for this tree in the second and third intervals.

D. IDENTIFYING THE VULNERABLE COMPONENTS

Using the probabilities obtained in the previous subsection, the storm-vulnerable components are identified. To this end, if the failure probability of a distribution branch in a time interval exceeds the vulnerability threshold, the distribution branch is recognized as vulnerable [29]. However, if a distribution branch fails in any time interval, the status of the distribution branch over the scheduling horizon (with N_T time intervals) is considered as damaged. This can be expressed in a compact form as follows:

$$\delta = \begin{cases} 0 & P_B^{f,\tau} \geq Tr \\ 1 & o.w. \end{cases} \quad \exists \tau \in \{1, 2, \ldots, N_T\} \quad (14)$$

Equation (14) ensures that if the failure probability of a branch at any time interval exceeds the vulnerability threshold, the branch is considered as a vulnerable branch to the upcoming windstorm (i.e. $\delta = 0$).

IV. PROBLEM FORMULATION

In this section, the mathematical formulation for optimal formation of islands is provided. This section employs the isolation constraints developed in previous section. In the optimization problem, the linear version of DistFlow equations is utilized as power flow equations [46]. In order to measure the resilience level of DSs, the priority-weighted supplied energy is employed in this paper, which includes both the load lost and its duration. In addition, the analysis in this study is conducted in steady-state condition. However, there are several resilience measures [47], which address different aspects of power systems under extreme events.

A. OBJECTIVE FUNCTION

The objective function of the proposed deterministic framework consists of two terms as follows:

$$F^{obj} = Max(\varepsilon_1 . \sum_{\forall cl} \sum_{\forall t} (P_{cl,t}^D - P_{cl,t}^{sh}) . D_{cl} - \varepsilon_2 . \sum_{\forall ij} \sum_{\forall \tau} (\alpha_{ij}^b . P_{ij}^{f,N_T})) \quad (15)$$

The objective of the optimization model is to maximize the priority-weighted value of the energy supplied to the critical loads, while the vulnerability of energized distribution branches during a storm is minimized. Each objective term is normalized by its maximum value, and the coefficients of objective terms are selected so that $\varepsilon_2 \ll \varepsilon_1$.

B. CONSTRAINTS

The optimization problem satisfies five groups of constraints, namely component isolation, load curtailment limits, power flow equations, island radial operation, and island connectivity constraints, which are listed as follows:

$$0 \leq \alpha_{ij}^b \leq \delta_{ij} \quad \forall ij \in \Omega_B \quad (16a)$$

$$0 \leq \alpha_{j}^b \leq \delta_{ij} \quad \forall ij \in \Omega_B \quad (16b)$$

$$0 \leq P_{i,t}^D - P_{i,t}^{sh} \leq M . \alpha_i^{cl} \quad \forall i \in \Omega_{CL},\ \forall t \quad (16c)$$

$$0 \leq Q_{i,t}^D - Q_{i,t}^{sh} \leq M . \alpha_i^{cl} \quad \forall i \in \Omega_{CL},\ \forall t \quad (16d)$$

$$0 \leq P_{i,t}^{sh}, Q_{i,t}^{sh} \quad \forall i \in \Omega_{CL},\ \forall t \quad (16e)$$

$$P_{i,t}^G - P_{i,t}^D + P_{i,t}^{sh} = \sum_{\forall ij}^{P_{ij,t}} \quad \forall i \in \Omega_N,\ \forall t \quad (16f)$$

$$Q_{i,t}^G - Q_{i,t}^D + Q_{i,t}^{sh} = \sum_{\forall ij} Q_{ij,t} \quad \forall i \in \Omega_N,\ \forall t \quad (16g)$$

$$-M.(1 - \alpha_{ij}^b) \leq V_{i,t} - V_{j,t} - \frac{r_{ij}.P_{ij,t} + x_{ij}.Q_{ij,t}}{V_0} \leq M.(1 - \alpha_{ij}^b) \quad \forall ij \in \Omega_B,\ \forall t \quad (16h)$$

$$V_i^{\min} . \alpha_i^n \leq V_{i,t} \leq V_i^{\max} . \alpha_i^n \quad \forall i \in \Omega_N,\ \forall t \quad (16i)$$

$$-P_{ij}^{\max} . \alpha_{ij}^b \leq P_{ij,t} \leq P_{ij}^{\max} . \alpha_{ij}^b \quad \forall ij \in \Omega_B,\ \forall t \quad (16j)$$

$$-Q_{ij}^{\max} . \alpha_{ij}^b \leq Q_{ij,t} \leq Q_{ij}^{\max} . \alpha_{ij}^b \quad \forall ij \in \Omega_B,\ \forall t \quad (16k)$$

$$P_i^{G,\min} . \alpha_i^g \leq P_{i,t}^G \leq P_i^{G,\max} . \alpha_i^g \quad \forall i \in \Omega_{DER},\ \forall t \quad (16l)$$

$$Q_i^{G,\min} . \alpha_i^g \leq Q_{i,t}^G \leq Q_i^{G,\max} . \alpha_i^g \quad \forall i \in \Omega_{DER},\ \forall t \quad (16m)$$

Vulnerable branches are isolated by (16a). If branch ij is recognized as vulnerable, it must be de-energized during storm ($\alpha_{ij}^b = 0$). Likewise, constraint (16b) de-energizes the ending nodes of the vulnerable switchable branches that have sectionalizing switches at their sending end. Constraints (16c) and (16d) set the active/reactive value of load curtailment to the amount of active/reactive loads for de-energized loads ($\alpha_i^{cl} = 0$). For the energized loads, these constraints ensure that the amount of active/reactive load curtailment must not exceed the total active/reactive load at each time interval. In (16c) and (16d), M is a large positive real number [48]. In addition, the active/reactive load shedding must be equal or greater than zero, which is ensured by (16e). Active and reactive power balances at each node are respectively enforced by equality constraints (16f) and (16g). In these two

equations, the active/reactive load curtailments and the power generated by distributed energy resources (DERs) are taken into account.

Constraint (16h) expresses the relationship between the voltage magnitudes of two connected nodes. However, note that the energization status of nodes and branches has not been determined before solving the optimization problem. Therefore, the big-M approach [49] is utilized in (16h) to guarantee that (16h) is only applied to the nodes connected through an energized branch. However, when the branch is not energized ($\alpha_{ij}^{b} = 0$), (16h) is relaxed for related nodes of i and j. In this constraint, V_0 stands for the reference voltage. Inequality constraint (16i) sets the voltage magnitude of a de-energized node ($\alpha_{i}^{n} = 0$) to zero and maintains the voltage magnitude within the acceptable bounds when the node is energized. Constraints (16j) and (16k) set the active/reactive flow of a de-energized line to zero, respectively. In addition, these constraints put limits on active/reactive power flow of each energized line. Constraints (16l) and (16m) ensure that only the committed DERs can inject power to the network. In addition, the active/reactive power outputs of the committed dispatchable DERs are respectively restricted by (16l) and (16m). The connectivity and island radial operation constraints, as configuration-related constraints, are taken into account in this paper. To this end, the connectivity and island radial operation constraints of [50] and [51] are utilized.

By solving this optimization problem, the optimal values of the unknown variables are determined, which are: the branch operational status, the node energization status, the load energization status, the node voltage magnitude, the active/reactive power flowing from node i to node j through branch ij, the active/reactive power generated by DERs, the commitment status of the dispatchable DERs, and the active/reactive amount of load shedding.

V. AN APPROACH FOR UNCERTAINTY MODELING AND MER ALLOCATION

The developed optimization model in (15) and (16) is deterministic, and it does not take uncertainties into account. To account for uncertain parameters in the developed model, a more complex formulation should be employed. Thus, a two-stage stochastic programming approach is employed in order to model the uncertainty associated with load demands. In addition, this framework allocates MERs before storm arrival. There are two groups of decisions to be taken in this problem, as summarized in the following:

The first-stage (here-and-now) variables: The optimal values of these variables are determined prior to the realization of the scenarios, and accordingly the decisions are implemented before storm arrival. In/out status of branches, on/off status of dispatchable DERs and MERs, energization status of nodes, voltage magnitude of nodes, active/reactive power flowing through branches, amount of active/reactive load shedding at each load point, amount of active/reactive power generated by DERs and MERs, and the variables related to MER allocation are determined before a storm strikes. Thus, the configurations of the constructed islands are determined before the strike of an upcoming storm.

The second-stage (wait-and-see) variables: After the uncertain parameters are revealed, the variables associated with the realized scenario are implemented. In this study, except for MER allocation variables, the second-stage variables are similar to the first-stage variables. Nonetheless, they are optimally determined for each scenario under study.

A. STOCHASTIC PROBLEM FORMULATION

Based on the discussions presented in the last section, the general expression of the two-stage stochastic framework is as follows:

$$\begin{aligned} &\text{Maximize } F^{obj} \\ &s.t. \begin{cases} (16a)-(16m), (19) & \omega = 1 \\ (20a)-(20p) & \omega = 2 \end{cases} \end{aligned} \tag{17}$$

Constraints (16a)-(16m) combined with constraint (19) guarantee the feasibility of solutions in the first stage ($\omega = 1$) of the two-stage stochastic optimization problem. In addition, constraints (20a)-(20p) are associated with the second stage ($\omega = 2$) of the stochastic problem. The constraints (20o) and (20p) are related to the operational constraints of the allocated MERs in the second stage of the stochastic problem.

1) OBJECTIVE FUNCTION

Similar to (15), the objective function of the stochastic problem includes two terms. The first objective term aims at maximizing the expected value of the energy supplied to the critical loads. On the other hand, the second one tends to minimize the expected vulnerability of the energized branches during a storm. The objective function of this problem is given as:

$$\begin{aligned} F^{obj} = Max(&\varepsilon_1 . \sum_{\forall s} \mu_s . \sum_{\forall cl} \sum_{\forall t} (P_{cl,t}^{D,s} - P_{cl,t}^{sh,s}) . D_{cl} \\ &- \varepsilon_2 . \sum_{\forall s} \mu_s . \sum_{\forall ij} \sum_{\forall \tau} (\alpha_{ij}^{b,s} . P_{ij}^{f,\tau})) \end{aligned} \tag{18}$$

In (18), μ_s accounts for the occurrence probability of scenario s.

2) CONSTRAINTS

a: FIRST-STAGE CONSTRAINTS

This set of constraints encompasses two categories, namely constraints (16a)-(16m) and constraint (19).

$$\sum_{\forall i} \psi_{m,i} \leq 1 \quad \forall m \in \Omega_{MER} \tag{19}$$

Constraint (19) is related to MER allocation and specifies that each MER cannot be allocated to more than one candidate node.

b: SECOND-STAGE CONSTRAINTS

The constraints of the second stage are imposed on each scenario, and they are expressed as follows:

$$0 \le \alpha_{ij}^{b,s} \le \delta_{ij} \quad \forall ij \in \Omega_B,\ \forall s \tag{20a}$$

$$0 \le \alpha_{j}^{b,s} \le \delta_{ij} \quad \forall ij \in \Omega_B,\ \forall s \tag{20b}$$

$$0 \le P_{i,t}^{D,s} - P_{i,t}^{sh,s} \le M.\alpha_i^{cl,s} \quad \forall i \in \Omega_{CL},\ \forall t, s \tag{20c}$$

$$0 \le Q_{i,t}^{D,s} - Q_{i,t}^{sh,s} \le M.\alpha_i^{cl,s} \quad \forall i \in \Omega_{CL},\ \forall t, s \tag{20d}$$

$$0 \le P_{i,t}^{sh,s}, Q_{i,t}^{sh,s} \quad \forall i \in \Omega_{CL},\ \forall t, s \tag{20e}$$

$$P_{i,t}^{G,s} - P_{i,t}^{D,s} + P_{i,t}^{sh,s} = \sum_{\forall ij} P_{ij,t}^{s} \quad \forall i \in \Omega_N,\ \forall t, s \tag{20f}$$

$$Q_{i,t}^{G,s} - Q_{i,t}^{D,s} + Q_{i,t}^{sh,s} = \sum_{\forall ij} Q_{ij,t}^{s} \quad \forall i \in \Omega_N,\ \forall t, s \tag{20g}$$

$$-M.(1-\alpha_{ij}^{b,s}) \le V_{i,t}^{s} - V_{j,t}^{s} - \frac{r_{ij}.P_{ij,t}^{s} + x_{ij}.Q_{ij,t}^{s}}{V_0} \le M.(1-\alpha_{ij}^{b,s}) \quad \forall ij \in \Omega_B, \forall t, s \tag{20h}$$

$$V_i^{\min}.\alpha_i^{n,s} \le V_{i,t}^{s} \le V_i^{\max}.\alpha_i^{n,s} \quad \forall i \in \Omega_N,\ \forall t, s \tag{20i}$$

$$-P_{ij}^{\max}.\alpha_{ij}^{b,s} \le P_{ij,t}^{s} \le P_{ij}^{\max}.\alpha_{ij}^{b,s} \quad \forall ij \in \Omega_B,\ \forall t, s \tag{20j}$$

$$-Q_{ij}^{\max}.\alpha_{ij}^{b,s} \le Q_{ij,t}^{s} \le Q_{ij}^{\max}.\alpha_{ij}^{b,s} \quad \forall ij \in \Omega_B,\ \forall t, s \tag{20k}$$

$$P_i^{G,\min}.\alpha_i^{g,s} \le P_{i,t}^{G,s} \le P_i^{G,\max}.\alpha_i^{g,s} \quad \forall i \in \Omega_{DER},\ \forall t, s \tag{20l}$$

$$Q_i^{G,\min}.\alpha_i^{g,s} \le Q_{i,t}^{G,s} \le Q_i^{G,\max}.\alpha_i^{g,s} \quad \forall i \in \Omega_{DER},\ \forall t, s \tag{20m}$$

$$0 \le \alpha_{m,i}^{g,s} \le \psi_{m,i} \quad \forall i \in \Omega_N,\ \forall m \in \Omega_{MER},\ \forall s \tag{20n}$$

$$P_m^{G,\min}.\alpha_{m,i}^{g,s} \le P_{m,i,t}^{G,s} \le P_m^{G,\max}.\alpha_{m,i}^{g,s} \quad \forall i \in \Omega_N,\ \forall m \in \Omega_{MER},\ \forall t, s \tag{20o}$$

$$Q_m^{G,\min}.\alpha_{m,i}^{g,s} \le Q_{m,i,t}^{G,s} \le Q_m^{G,\max}.\alpha_{m,i}^{g,s} \quad \forall i \in \Omega_N,\ \forall m \in \Omega_{MER},\ \forall t, s \tag{20p}$$

The explanation for constraints (20a)-(20m) is the same as (16a)-(16m). Constraint (20n) ensures that MER m can inject power to the network through node i if it is allocated to this node. The active and reactive output power of a committed MER ($\alpha_{m,i}^{g,s}$ =1) are respectively restricted by (20o) and (20p).

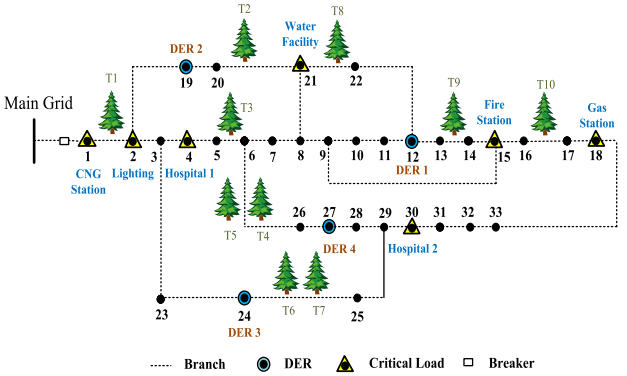

FIGURE 8. The 33-bus test system.

VI. NUMERICAL RESULTS

In this section, the proposed framework is implemented on the 33- and 123-bus distribution test systems, as well as a practical feeder through nine case studies. Fig. 8 shows the schematic representation of the 33-bus test system. The information about this test system can be found in [52].

A. TEST SYSTEMS AND ASSUMPTIONS

1) 33-BUS DISTRIBUTION SYSTEM

Six types of critical loads are considered in the test system. The critical loads are located at nodes 1, 2, 4, 15, 18, 21, and 30. Hourly load variations of these critical loads can be observed in [53]. As can be traced in Fig. 8, the grid includes four dispatchable DERs. The DERs are rated at 100 kW and 60 kVAr.

2) TREES

Ten trees are located adjacent to the distribution branches of the 33-bus test system. The proposed framework is general, and different types of trees can be considered in this framework. However, for the sake of simplicity, it is assumed that all of the trees are of the spruce species type (which is common in some countries, such as Finland and Norway). In addition, it is assumed that each tree has grown adjacent to the middle of its adjacent line-section. Tree height and distance from the distribution lines are listed in Table 1 [54]. It is assumed that height of all distribution lines is 10.5 m. The critical wind speeds for the uprooting and stem breakage of the spruce are assumed to be 37 and 46 m/s, respectively [55]. In the simulations, it is assumed that the values of κ and ζ are 0.3 and 0.6, respectively [36].

3) WINDSTORM

It is assumed that the windstorm hits the distribution system for three hours, and the duration of the windstorm is divided into three equal intervals. The maximum wind speed and wind direction for each interval are listed in Table 2. To identify the vulnerable branches, the vulnerability threshold of distribution branches is assumed to be 0.25.

TABLE 1. General information on trees and their locations.

Tree #	Adjacent Branch	Tree Height (m)	Distance (m)	ϑ_T
T1	1-2	18.5	14	1
T2	20-21	16	6	1
T3	5-6	18	14	1
T4	6-26	17	12	0
T5	6-26	17	10	1
T6	24-25	15	12	1
T7	24-25	15	12	1
T8	21-22	12	8	1
T9	13-14	11	6	1
T10	16-17	21	9	1

TABLE 2. Maximum wind-speed and direction of storm in each interval.

Interval #	Wind Speed (m/s)	Direction (deg)
1	35	259 ± 22
2	47	259 ± 22
3	40	259 ± 22

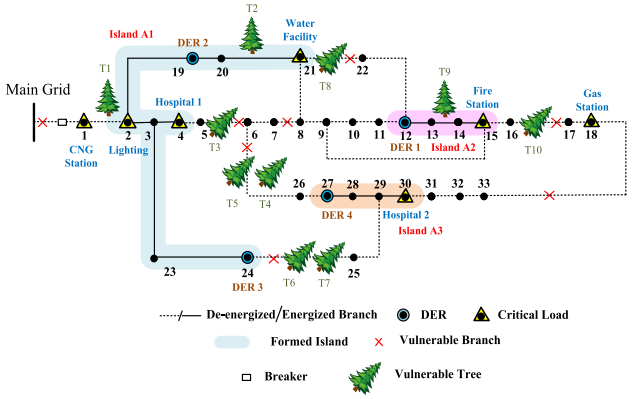

FIGURE 9. The constructed islands developed in case study I.

B. RESULTS AND DISCUSSION

Nine case studies are defined in order to explore the effectiveness of the proposed models. Without loss of generality, it is assumed that the upstream network is faulty during windstorm. The results of the simulations are expressed in terms of the priority-weighted supplied energy (SE) and vulnerable branches. In these simulations, the values of ε_1 and ε_2 are assumed to be 0.99 and 0.01, respectively.

Case Study I: Impacts of tree fall/breakage on island formation (*considering tree-caused failures*)

In this case study, both direct and indirect effects of windstorms on lines are considered, and islands are constructed prior to storm arrival. The islands are formed such that the priority-weighted curtailed energy is maximized. At the same time, the vulnerability of energized branches is minimized. Fig. 9 depicts the constructed islands.

The CNG station is not supplied by any DERs. It is due to the presence of tree T1 which is located adjacent to branch 1-2. Although tree T1 has not been identified vulnerable to the approaching storm, this configuration of island A1 is less vulnerable to the storm. Thus, branch 1-2 remains unenergized. Likewise, the gas station at bus 18 is isolated due to two vulnerable branches connected to it. The vulnerable branch 16-17 is threatened by tree T10. On the other hand, vulnerable branch 18-33 can directly be damaged by the windstorm. As a consequence, the gas station is not supplied through the formed islands.

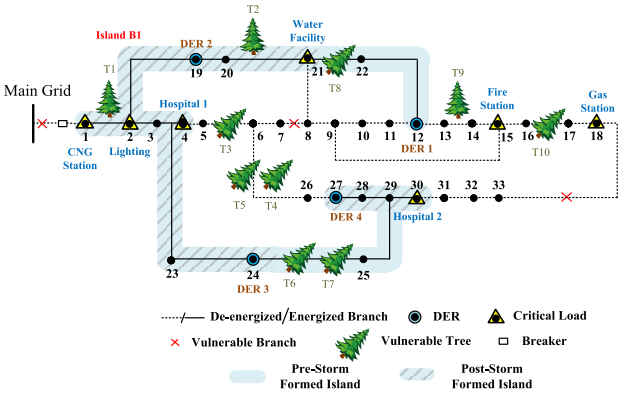

FIGURE 10. The constructed islands before and after windstorms in case study II.

As can be seen in Fig. 9, although tree T2 is not labeled as a storm-vulnerable tree, it may damage branch 20-21 during storm. However, the proposed framework serves the water station through island A1, and energizes this branch. The reason for this lies in the importance of the water facility in satisfying the basic needs of human life. As can be traced in Table 1, the fallen stem or branches of tree T4 would not touch branch 6-26 due to the wind direction. As a note, the computation time of this case study is 18 *s*.

Case Study II: Island formation where the tree-caused failures are ignored, and comparison of the results with Case Study I.

In this case study, the proposed framework is compared with a model in which the tree-caused failures are neglected. In other words, only direct effects of windstorms on distribution lines are considered. Obviously, the number of distribution branches recognized as vulnerable prior to windstorm in this case study is lower than case study I. In fact, two branches 7-8 and 18-33 are recognized as vulnerable, and the five tree-caused failures are neglected. The formed islands before and after the windstorm are shown in Fig. 10.

However, when the windstorm hits the DS, seven distribution branches are damaged in this case. The tree-induced faults occur at the beginning of the second time interval. In this condition, the protection systems of the DERs detect the faults, and the DERs are put out of service. Consequently, the critical loads are de-energized. In this condition, the repair crews are dispatched to the DS. They will find the fault locations first. Subsequently, the faulty branches are isolated form the rest of the DS. In doing so, the initially formed island is divided into two islands that are shown via the hatched area in Fig. 10. In the first island, DER 4 supplies hospital 2. Likewise, the water facility, lighting, CNG station, and hospital 1 are energized through DERs 2 and 3. Therefore, pre-storm formed island B1 cannot properly deal with the windstorm. The value of SE and vulnerable branches for case studies I and II are listed in Table 3. The value of

TABLE 3. Comparison between results of case studies I and II.

	Case I (considering tree-caused failures)	Case II (ignoring tree-caused failures)
SE(p.u.)	3.6379	2.3729
Vulnerable Branches	5-6, 7-8, 16-17, 21-22, 24-25, 6-26, 18-33	7-8, 18-33

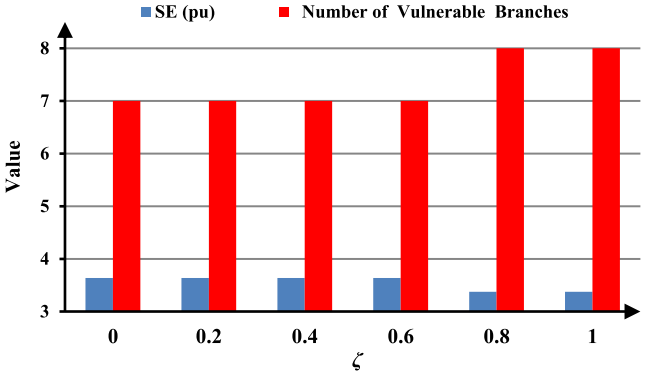

FIGURE 11. SE and number of vulnerable branches.

SE in case study I is 53.3 percent higher than SE in case study II. It should be notified that the faulty branches after the windstorm onset are the same for case studies I and II, and are equal to the vulnerable branches in case study I. The only difference lies in the pre-windstorm actions, which can prevent some post-windstorm load interruptions.

Case Study III: Sensitivity analysis on ζ.

In this case study, the impact of various values of ζ (fraction of tree stem that is broken by storm and falls down on the ground) is investigated. For a tree, this parameter is impacted by different factors, such as tree height and diameter [36]. Thus, the value of ζ is increased from zero to one. It means that a larger fraction of tree trunk is blown down by the windstorm. Thus, the probability that a branch is damaged by its adjacent tree trunk increases. In this situation, "stem breakage" makes greater contribution to tree-induced failure probability of distribution branches. The results of this study in terms of SE and the number of vulnerable branches are shown in Fig. 11.

When the value of ζ increases from 0 to 0.6, the amount of supplied energy and the number of vulnerable branches do not change. However, once it reaches 0.8 or higher, branch 1-2 is considered vulnerable, and it is added to the vulnerable branches. In this situation, eight branches can be damaged during the upcoming storm, and the value of supplied energy decreases from 3.6379 to 3.3737 pu. Despite the variation of ζ, the obtained results show low sensitivity to the value of this parameter. This observation can be justified as follows: for the spruce species, the critical wind speed for uprooting (37 m/s) is lower than that for stem breakage (46 m/s). Thus, it is highly probable that the trees are uprooted during storms. Indeed, the observations made during different storms confirm this observation [43]. In particular, when the value of ζ is equal to zero, only uprooted trees or broken branches can touch the lines. Thus, five lines are vulnerable under these failure modes of trees during the storm (in addition to two lines that

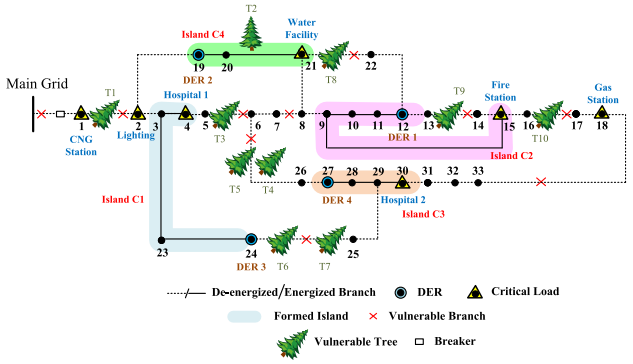

FIGURE 12. Constructed islands prior to the upcoming storm in case study IV.

TABLE 4. The results of case study IV.

SE (pu)	Vulnerable Branches
3.3737	1-2, 5-6, 7-8, 13-14, 16-17, 21-22, 24-25, 6-26, 18-33

can directly be damaged by the storm, as discussed in Case Study II). Regarding the tree heights and the distances given in Table 1, branch 1-2 is considered vulnerable if ζ exceeds 0.8. Thus, only for tree T1, stem breakage state can contribute to making branch 1-2 vulnerable to the approaching storm, and tree-caused failures will mainly occur due to uprooting.

Case Study IV: Impacts of the distances between the trees and their adjacent branches.

This case study investigates the impacts of the distances between the trees and distribution branches. To this end, all the distances given in Table 1 are decreased by 3 m. Other assumptions remain the same as Case Study I. Consequently, the number of vulnerable branches to the upcoming storm increases. Fig. 12 shows the constructed islands in this case.

As can be traced in Fig. 12, the distribution network is divided into four islands prior to storm arrival. Compared to Case Study I, branches 1-2 and 13-14 are added to the vulnerable branches, and they are de-energized. As a consequence of de-energization of these branches, island A1 (in Case Study I) is split into two islands C1 and C4. Furthermore, in island C2, the fire station is served via a longer path compared to island A2. This is because branch 13-14 is recognized as vulnerable to the upcoming storm. The amount of supplied energy as well as the number of vulnerable branches are listed in Table 4. The results of this study imply that the characteristics and locations of trees can considerably impact the network fault locations in distribution systems during wind storms, and they should be considered in proactive scheduling of islands against windstorms.

Case Study V: Impacts of the duration of time intervals.

In order to investigate the impacts of windstorm dynamic behavior, a sensitivity analysis in terms of the duration of storm time intervals is conducted. In fact, as the number of storm time intervals increases, more data on the storm speed variations and storm movement can be incorporated into the framework. As mentioned earlier, the upcoming storm will hit the region for 3 hours. In this case study, the duration of

TABLE 5. Maximum wind speeds for different time intervals.

Interval Number	Maximum Wind Speeds (m/s)											
1	47											
3	35				47				40			
6	32		35		40		47		40		39	
12	32	25	35	30	38	40	47	43	40	35	38	39

TABLE 6. The results of case study V.

Interval Number	1	3	6	12
Interval Duration (min)	180	60	30	15
Number of Vulnerable Branches	7	7	8	8
Number of Constraints	606	1434	2676	5164
Computation Time (s)	21	25	37	60
SE (pu)	3.6379	3.6379	3.5663	3.5663

the storm time intervals is changed. As the number of time intervals increases, their duration decreases. In each interval, the maximum forecasted wind speed is used. Subsequently, these wind speeds along with other required data are fed as inputs into the proposed framework. Table 5 shows the maximum wind speeds during the storm, considering four conditions for the number of time intervals during the storm.

The obtained results of this analysis in terms of SE, number of vulnerable branches, computation time, and number of constraints for each condition are reported in Table 6.

The results demonstrate that by decreasing the duration of time intervals, more information about storm dynamic is utilized by the framework. Thus, in this case, the size of problem increases. Nonetheless, as can be traced in Table 6, the computation time does not significantly rise. In addition, when the duration of interval is decreased from 180 to 15 min, the SE and number of vulnerable branches indicate small variation. This is because the maximum wind speeds are associated with storm-caused damages, and they are also included in the problem when the number of time intervals is low. Using the results of this analysis, the decision makers can divide the storm duration into a desired number of storm time intervals based on the available data, computational burden, and desired accuracy.

Case Study VI: Considering MER allocation and the uncertainty associated with load demands.

In this case study, the proposed stochastic framework in Section V is implemented on the 33-bus test system. The uncertainty associated with load demands is considered, and 200 initial scenarios for load demands are generated using the Monte Carlo simulation method [56]. To this end, it is assumed that load prediction errors follow normal distribution [57]. Their standard deviations are equal to 10% of the predicted values at each time interval. Subsequently, in order to reduce the computational complexity of the optimization problem, the initial scenarios are reduced to 10 final scenarios using the backward reduction algorithm [58]. It is assumed that there are two MER units available. The rated power for

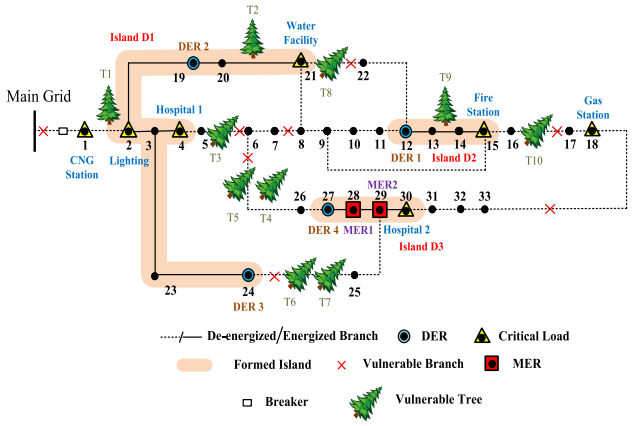

FIGURE 13. Constructed islands prior to the upcoming storm in case study VI.

TABLE 7. The results of case study VI.

	Stochastic Model without MER Allocation	Stochastic Model with MER Allocation
ESE(p.u.)	3.6089	4.1098
Vulnerable Branches	5-6, 7-8, 16-17, 21-22, 24-25, 6-26, 18-33	5-6, 7-8, 16-17, 21-22, 24-25, 6-26, 18-33

both MERs is 20 kW and 15 kVAr. The proposed two-stage stochastic framework is applied to the 33-bus test system, and the optimal values of the first- and second-stage variables are determined. Fig. 13 shows the constructed islands in the first stage of the proposed framework (i.e. ahead of coming storm).

As shown in Fig. 13, the two MERs are allocated to the nodes 28 and 29. The special reason for this allocation is the location of the two hospitals with respect to this distribution network. The electricity demand of the hospitals is relatively high if compared with the other critical loads of this system. However, the capacity of DER 4 is not sufficient to supply hospital 2, and even the curtailed load of hospital 2 is high. Furthermore, these hospitals have the highest priority factor among the existing critical loads in the system. On these bases, the two available MERs are allocated to the buses of island D3.The configurations of the pre-storm constructed islands in this case study is the same as Case Study I. Because, the characteristics of the storm, DS components, and the trees are the same for both case studies, and these factors determine the locations of vulnerable branches. In contrast, the optimal values of other variables differ in these two case studies.

To determine the impact of MER allocation, the proposed stochastic framework is run another time without MER allocation. The results of this comparison in terms of the expected supplied energy (ESE) and vulnerable branches are presented in Table 7.

The results for the case with MER allocation show the great advantages of MER allocation in the face of storms. In this study, although the capacity of MERs is small (20 kW), the ESE is improved by 13.87 percent. The reason is that the available MERs are allocated to the nodes (28 and 29) that make greater contribution to the value of priority-weighted supplied energy after storm onset.

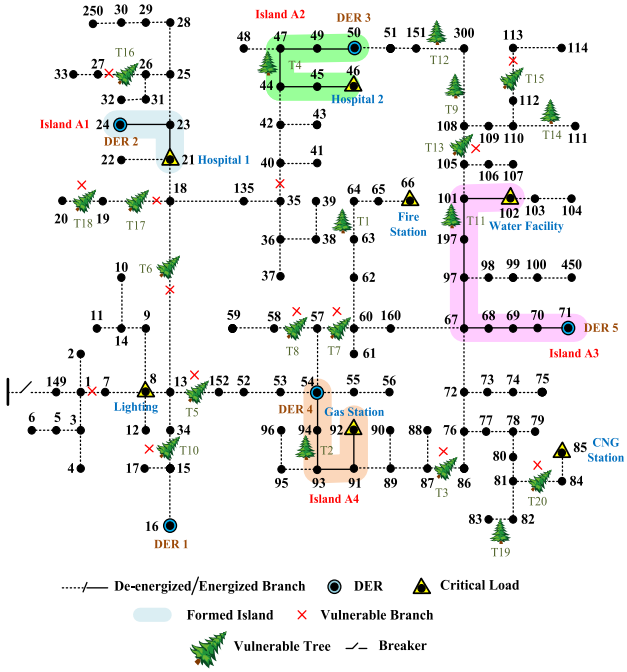

FIGURE 14. Constructed islands prior to the upcoming storm in case study VII.

TABLE 8. The results of case study VII.

SE (pu)	Vulnerable Branches
3.3296	1-7, 13-18, 18-19, 19-20, 15-34, 26-27, 35-40, 57-58, 57-60, 81-84, 86-87, 105-108, 112-113, 13-152

Case Study VII: Implementing the framework on the 123-node distribution test feeder.

In order to implement the proposed deterministic framework on a large practical system, the IEEE 123-bus test system is employed [59]. There are five DERs in the test system. For the sake of simplicity, the characteristics of trees T11-T20 are respectively assumed similar to those of trees T1-T10 (i.e. T11 is identical to T1, T12 is identical to T2, etc). Other assumptions are the same as Case Study I. By implementing the proposed framework on the test system, four islands are constructed before storm arrival, which are shown in Fig. 14.

In addition, 14 distribution branches are identified as vulnerable, and they are proactively de-energized, which can be observed in Table 8. The value of SE is also reported in this table.

As can be seen in Fig. 14, DER1 is isolated from the grid and cannot inject power into the DS. The reason is the vulnerability of branch 15-34. Similarly, the fire station, lighting, and CNG station are isolated from the rest of the system, and they are not supplied by any DERs. The computation time for this case study is 42 *s,* which confirms the computation time efficiency of the proposed model for large distribution grids.

Case Study VIII: Implementing the framework on an existing distribution feeder.

In this part, in order to explore the performance of the proposed framework on a practical distribution network, a large feeder of a distribution utility company in Iran is utilized. The single line diagram of the feeder under study is shown in Fig. 15.

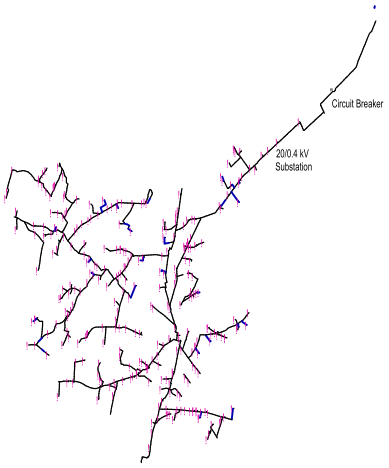

FIGURE 15. Single-line diagram of the practical distribution feeder under study in case study VIII (pink circles denote 20/0.4 kV substations).

TABLE 9. The results of case study VIII.

	Considering tree-caused failures	Ignoring tree-caused failures
SE(p.u.)	2.232	1.259
Number of Vulnerable Lines	29	6

This feeder includes 279 load points. In addition, 1656 trees have grown near the overhead lines. The tree heights range from 6 m to 31.6 m. The species of the trees are Platanus, locust, and white poplar. There are three DERs in the feeder. Other assumptions and information are similar to Case study I. The proposed framework is tested on the distribution network. The results in terms of SE and number of vulnerable lines are given in Table 9.

The results imply that when the tree-caused failures are considered, 29 line sections are vulnerable to the upcoming storm. In addition, the value of SE is 77.3 percent higher than the condition in which only direct effects of storms are taken into account. When the trees are ignored, the distribution company predicts six power outages in the feeder. However, once the storm strikes the feeder, 29 distribution lines are damaged by the storm and the trees. Thus, the distribution company cannot properly supply the critical loads based on its restoration strategy. Nonetheless, the proposed framework predicts all the storm-related outages, and accordingly constructs the islands. Thus, the value of SE is improved.

Although the species of the trees in this case study have larger branches with respect to the spruce, the tree trimming programs are regularly performed by the company, in particular in autumns and springs. Thus, tree-caused failures due to branch breakage can be controlled. The trees may mainly threaten their adjacent lines via uprooting and stem breakage damage modes. In addition, the constructed islands serve the local critical loads after the storm strikes. The computation time for the distribution network is 223 *s*, which

TABLE 10. Different scenarios for the maximum wind speed at each time interval of the storm (m/s).

	t=1	t=2	t=3
Scenario 1	29	36	34
Scenario 2	29	38	34
Scenario 3	35	47	40
Scenario 4	39	51	44

TABLE 11. The results for different wind speed scenarios.

	SE (pu)	Number of Vulnerable Branches
Scenario 1	5.6485	0
Scenario 2	4.5	8
Scenario 3	3.3296	14
Scenario4	2.1	29

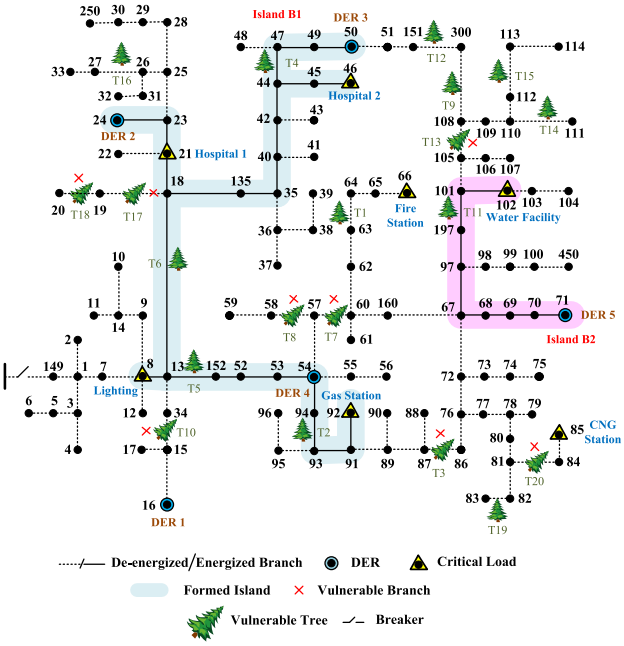

FIGURE 16. Constructed islands prior to the upcoming storm for scenario 2 of wind speed profile.

clearly verifies the computational tractability of the proposed framework for large DSs with a large number of trees. This is because the trees and their characteristics do not impact the size of the optimization problem. However, they determine the vulnerable lines, and these lines are used as inputs of the optimization problem for island formation. Furthermore, this computation time is significantly smaller than the time available for making decisions before storm arrival.

Case Study IX: Impacts of different wind speed profiles.

In this case study, four different wind speed profiles are employed for the storm. Subsequently, the maximum wind speed at each time interval is determined and is used as the input to the proposed deterministic framework. Table 10 shows the maximum wind speeds for each scenario.

Using the data of Table 10, the proposed deterministic framework is implemented on the IEEE 123-bus test system for each of the wind speed scenarios, while the other assumptions are the same as those in the Case Study VII. The results of the simulation, in terms of the supplied energy and the number of storm-vulnerable branches, are determined and reported in Table 11.

As can be seen in Table 11, maximum wind speeds have considerable impacts on the results. Thus, the wind speed profile is an important input parameter of the models. In this regard, forecasting the weather features of the approaching windstorms plays a significant role in the preparedness measures in DSs. For example, in scenario 2, eight distribution branches are recognized as vulnerable to the upcoming storm, and accordingly the suitable islands are constructed, which are different from the islands constructed under scenario 3 (Case Study VII). The configurations of the islands developed under scenario 2 are depicted in Fig. 16.

As can be traced in Fig. 16, island B1 in this case study includes islands A1, A2, and A4 of Case Study VII. In addition, the street lighting is supplied via island B1. Therefore, the amount of SE is increased to 4.5 pu. Based on the results of this case study, the decision-makers can explore the impacts of different wind speed profiles on the required preparedness measures, and how to form the islands based on preferred conservativeness level.

VII. SUMMARY AND CONCLUSION

This paper proposes a new framework for incorporating tree failure modes into the restoration of critical loads in the case of windstorms. A new discrete Markov chain is developed that simulates the response of a tree during a time interval of storm duration. In addition, a novel line-tree interaction model is proposed for quantifying the impacts of each tree failure mode on its adjacent distribution lines. The proactive island formation was modeled as a MILP optimization problem. Subsequently, a two-stage stochastic framework is proposed in order to characterize the uncertainty associated with load demands. This stochastic framework considers MER allocation problem as well.

The proposed models are implemented on two distribution test systems and a practical distribution feeder through nine case studies. In each case study, storm-vulnerable branches are identified, and they are de-energized. Thus, the systems are sectionalized into a number of islands prior to windstorms. Moreover, the results of the proposed framework are compared with a model in which the effects of tree fall and breakage are ignored. The comparison shows 53.3 percent improvement in the amount of supplied energy to the critical loads. A sensitivity analysis was conducted in order to explore the impact of ζ on the results. These results and comparison demonstrate how trees contribute to the distribution line failures during windstorms through different mechanisms. In addition, a sensitivity analysis on the number of storm intervals was performed to determine how the simulation results and complexity will change if more data about storms are available. Based on the results of this analysis, the decision makers can make a tradeoff between computational burden and solution accuracy. Furthermore, the simulation results indicate that using the proposed models for characterizing tree failure modes, the decision makers

can more realistically evaluate the vulnerability of overhead distribution lines to windstorms. Thus, operation-oriented measures, such as MER allocation, can be done in a way that the supplied energy is maximized. Future work will focus on planning strategies for DS resilience enhancement. In particular, optimal sectionalizing switch placement in DSs and optimal expansion of DSs will be studied when the tree-caused failures are taken into account.

ACKNOWLEDGMENT

The authors would like to thank "Alborz Electricity Distribution Company" for providing the detailed information on an existing distribution network of their grid and the information about the plants surrounding the overhead lines of this network, which helped them to carry out Case Study VIII, and also would like to thank Dr. Khan Beigy from the research department, and to Dehghan from the operation department of this company for their cooperation.

REFERENCES

[1] S. Oh, K. Heo, F. H. Jufri, M. Choi, and J. Jung, "Storm-induced power grid damage forecasting method for solving low probability event data," *IEEE Access*, vol. 9, pp. 20521–20530, 2021.
[2] F. Yang, P. Watson, M. Koukoula, and E. N. Anagnostou, "Enhancing weather-related power outage prediction by event severity classification," *IEEE Access*, vol. 8, pp. 60029–60042, 2020.
[3] M. Mohammadian, F. Aminifar, N. Amjady, and M. Shahidehpour, "Data-driven classifier for extreme outage prediction based on Bayes decision theory," *IEEE Trans. Power Syst.*, vol. 36, no. 6, pp. 4906–4914, Nov. 2021.
[4] M. Bahrami, M. Vakilian, H. Farzin, and M. Lehtonen, "Pre-flooding island formation in distribution systems resolving local critical infrastructures interdependency," in *Proc. 25th Elect. Power Distrib. Conf. (EPDC)*, 2021, pp. 5–10.
[5] E. Kabir, S. D. Guikema, and S. M. Quiring, "Predicting thunderstorm-induced power outages to support utility restoration," *IEEE Trans. Power Syst.*, vol. 34, no. 6, pp. 4370–4381, Nov. 2019.
[6] S. Hartling, V. Sagan, M. Maimaitijiang, W. Dannevik, and R. Pasken, "Estimating tree-related power outages for regional utility network using airborne LiDAR data and spatial statistics," *Int. J. Appl. Earth Observ. Geoinf.*, vol. 100, Aug. 2021, Art. no. 102330.
[7] EPRI. *Distribution Grid Resiliency: Overhead Structures*. Accessed: Oct. 15, 2021. [Online]. Available: https://www.epri.com/research/products/000000003002006780
[8] D. F. D'Amico, S. M. Quiring, C. M. Maderia, and D. B. McRoberts, "Improving the hurricane outage prediction model by including tree species," *Climate Risk Manage.*, vol. 25, Jan. 2019, Art. no. 100193.
[9] S. Yuan, S. M. Quiring, L. Zhu, Y. Huang, and J. Wang, "Development of a typhoon power outage model in Guangdong, China," *Int. J. Elect. Power Energy Syst.*, vol. 117, May 2020, Art. no. 105711.
[10] E. Kabir, S. Guikema, and B. Kane, "Statistical modeling of tree failures during storms," *Rel. Eng. Syst. Saf.*, vol. 177, pp. 68–79, Sep. 2018.
[11] B. Gardiner, K. Byrne, S. Hale, K. Kamimura, S. J. Mitchell, H. Peltola, and J.-C. Ruel, "A review of mechanistic modelling of wind damage risk to forests," *Forestry*, vol. 81, no. 3, pp. 447–463, Jul. 2008.
[12] H. Peltola, S. Kellomäki, H. Väisänen, and V.-P. Ikonen, "A mechanistic model for assessing the risk of wind and snow damage to single trees and stands of Scots pine, Norway spruce, and birch," *Can. J. Forest Res.*, vol. 29, no. 6, pp. 647–661, Jun. 1999.
[13] P. Ancelin, B. Courbaud, and T. Fourcaud, "Development of an individual tree-based mechanical model to predict wind damage within forest stands," *Forest Ecol. Manage.*, vol. 203, pp. 101–121, Dec. 2004.
[14] E. Hart, K. Sim, K. Kamimura, C. Meredieu, D. Guyon, and B. Gardiner, "Use of machine learning techniques to model wind damage to forests," *Agricult. Forest Meteorol.*, vol. 265, pp. 16–29, Feb. 2019.
[15] K. Kamimura, B. Gardiner, S. Dupont, D. Guyon, and C. Meredieu, "Mechanistic and statistical approaches to predicting wind damage to individual maritime pine (*Pinus pinaster*) trees in forests," *Can. J. Forest Res.*, vol. 46, no. 1, pp. 88–100, 2016.
[16] D. T. Radmer, P. A. Kuntz, R. D. Christie, S. S. Venkata, and R. H. Fletcher, "Predicting vegetation-related failure rates for overhead distribution feeders," *IEEE Trans. Power Del.*, vol. 17, no. 4, pp. 1170–1175, Oct. 2002.
[17] D. W. Wanik, J. R. Parent, E. N. Anagnostou, and B. M. Hartman, "Using vegetation management and LiDAR-derived tree height data to improve outage predictions for electric utilities," *Electr. Power Syst. Res.*, vol. 146, pp. 236–245, May 2017.
[18] S. D. Guikema, R. A. Davidson, and H. Liu, "Statistical models of the effects of tree trimming on power system outages," *IEEE Trans. Power Del.*, vol. 21, no. 3, pp. 1549–1557, Jul. 2006.
[19] C. Zhai, T. Y.-J. Chen, A. G. White, and S. D. Guikema, "Power outage prediction for natural hazards using synthetic power distribution systems," *Rel. Eng. Syst. Saf.*, vol. 208, Apr. 2021, Art. no. 107348.
[20] R. Nateghi, S. Guikema, and S. M. Quiring, "Power outage estimation for tropical cyclones: Improved accuracy with simpler models," *Risk Anal.*, vol. 34, no. 6, pp. 1069–1078, Jun. 2014.
[21] H. Hou, S. Zhu, H. Geng, M. Li, Y. Xie, L. Zhu, and Y. Huang, "Spatial distribution assessment of power outage under typhoon disasters," *Int. J. Electr. Power Energy Syst.*, vol. 132, Nov. 2021, Art. no. 107169.
[22] G. Li, P. Zhang, P. B. Luh, W. Li, Z. Bie, C. Serna, and Z. Zhao, "Risk analysis for distribution systems in the northeast U.S. Under wind storms," *IEEE Trans. Power Syst.*, vol. 29, no. 2, pp. 889–898, Nov. 2013.
[23] D. Cerrai, D. W. Wanik, M. A. E. Bhuiyan, X. Zhang, J. Yang, M. E. B. Frediani, and E. N. Anagnostou, "Predicting storm outages through new representations of weather and vegetation," *IEEE Access*, vol. 7, pp. 29639–29654, 2019.
[24] M. E. Parast, M. H. Nazari, and S. H. Hosseinian, "Resilience improvement of distribution networks using a two-stage stochastic multi-objective programming via microgrids optimal performance," *IEEE Access*, vol. 9, pp. 102930–102952, 2021.
[25] Y. Du, X. Lu, J. Wang, and S. Lukic, "Distributed secondary control strategy for microgrid operation with dynamic boundaries," *IEEE Trans. Smart Grid*, vol. 10, no. 5, pp. 5269–5282, Sep. 2019.
[26] Z. Ye, C. Chen, B. Chen, and K. Wu, "Resilient service restoration for unbalanced distribution systems with distributed energy resources by leveraging mobile generators," *IEEE Trans. Ind. Informat.*, vol. 17, no. 2, pp. 1386–1396, Feb. 2021.
[27] K. Sandhya, T. Ghose, D. Kumar, and K. Chatterjee, "PN inference based autonomous sequential restoration of distribution system under natural disaster," *IEEE Syst. J.*, vol. 14, no. 4, pp. 5160–5171, Dec. 2020.
[28] K. S. A. Sedzro, X. Shi, A. J. Lamadrid, and L. F. Zuluaga, "A heuristic approach to the post-disturbance and stochastic pre-disturbance microgrid formation problem," *IEEE Trans. Smart Grid*, vol. 10, no. 5, pp. 5574–5586, Sep. 2019.
[29] M. H. Amirioun, F. Aminifar, and H. Lesani, "Resilience-oriented proactive management of microgrids against windstorms," *IEEE Trans. Power Syst.*, vol. 33, no. 4, pp. 4275–4284, Jul. 2018.
[30] M. H. Amirioun, F. Aminifar, and H. Lesani, "Towards proactive scheduling of microgrids against extreme floods," *IEEE Trans. Smart Grid*, vol. 9, no. 4, pp. 3900–3902, Jul. 2018.
[31] S. Ma, B. Chen, and Z. Wang, "Resilience enhancement strategy for distribution systems under extreme weather events," *IEEE Trans. Smart Grid*, vol. 9, no. 2, pp. 1442–1451, Mar. 2018.
[32] D. Boucher, C. Rodick, J. Bailey, J. Snitzer, K. Kyde, and B. Prudden, "Hurricane Isabel and the forests of the mid-Atlantic Piedmont and blue ridge: Short-term impacts and long-term implications," in *Hurricane Isabel in Perspective*, K. G. Sellner, Ed. Edgewater, MD, USA: Chesapeake Res. Consortium, 2005, pp. 5–160.
[33] D. N. Trakas and N. D. Hatziargyriou, "Optimal distribution system operation for enhancing resilience against wildfires," *IEEE Trans. Power Syst.*, vol. 33, no. 2, pp. 2260–2271, Mar. 2018.
[34] A. M. Salman, Y. Li, and M. G. Stewart, "Evaluating system reliability and targeted hardening strategies of power distribution systems subjected to hurricanes," *Rel. Eng. Syst. Saf.*, vol. 144, no. 3, pp. 319–333, Dec. 2015.
[35] R. Billinton and R. N. Allan, *Reliability Evaluation of Engineering Systems*. New York, NY, USA: Plenum Press, 1992.
[36] R. Seidl, W. Rammer, and K. Blennow, "Simulating wind disturbance impacts on forest landscapes: Tree-level heterogeneity matters," *Environ. Model. Softw.*, vol. 51, pp. 1–11, Jan. 2014.
[37] R. A. Davidson, H. Liu, and T. V. Apanasovich, "Estimation of post-storm restoration times for electric power distribution systems," in *Advances in Electric Power and Energy Systems*. Hoboken, NJ, USA: Wiley, Jun. 2017, p. 251.

[38] C. Ciftci, S. R. Arwade, B. Kane, and S. F. Brena, "Analysis of the probability of failure for open-grown trees during wind storms," *Probabilistic Eng. Mech.*, vol. 37, pp. 41–50, Jul. 2014.
[39] C. D. Canham, M. J. Papaik, and E. F. Latty, "Interspecific variation in susceptibility to windthrow as a function of tree size and storm severity for northern temperate tree species," *Can. J. Forest Res.*, vol. 31, no. 1, pp. 1–10, Jan. 2001.
[40] F. Cadini, G. L. Agliardi, and E. Zio, "A modeling and simulation framework for the reliability/availability assessment of a power transmission grid subject to cascading failures under extreme weather conditions," *Appl. Energy*, vol. 185, pp. 267–279, Jan. 2017.
[41] EPRI. *Impacts of Extreme Weather Events on Transmission and Distribution Systems: Case Histories, Lessons Learned and Good Practices*. Accessed: Feb. 222, 2022. [Online]. Available: https://www.epri.com/research/products/000000000001020145
[42] *Hurricane Michael: Unprecedented Storm, Unprecedented Response*, Gulf Power Company, Pensacola, FL, USA, 2018.
[43] (2020). *A Violent Thunder Front Caused Devastation in Several Areas on Friday Night in North Karelia*. [Online]. Available: https://yle.fi/uutiset/3-11421818.
[44] A. Papoulis, *Probability, Random Variables, and Stochastic Processes*. New York, NY, USA: McGraw-Hill, 1991, pp. 345–348.
[45] M. Nazemi, M. Moeini-Aghtaie, M. Fotuhi-Firuzabad, and P. Dehghanian, "Energy storage planning for enhanced resilience of power distribution networks against earthquakes," *IEEE Trans. Sustain. Energy*, vol. 11, no. 2, pp. 795–806, Apr. 2020.
[46] H.-G. Yeh, D. F. Gayme, and S. H. Low, "Adaptive VAR control for distribution circuits with photovoltaic generators," *IEEE Trans. Power Syst.*, vol. 27, no. 3, pp. 1656–1663, Aug. 2012.
[47] S. Talukder, M. Ibrahim, and R. Kumar, "Resilience indices for power/cyberphysical systems," *IEEE Trans. Syst., Man, Cybern., Syst.*, vol. 51, no. 4, pp. 2159–2172, Apr. 2021.
[48] T. Ding, R. Bo, W. Gu, and H. Sun, "Big-M based MIQP method for economic dispatch with disjoint prohibited zones," *IEEE Trans. Power Syst.*, vol. 29, no. 2, pp. 976–977, Mar. 2014.
[49] T. Ding, K. Sun, C. Huang, Z. Bie, and F. Li, "Mixed-integer linear programming-based splitting strategies for power system islanding operation considering network connectivity," *IEEE Syst. J.*, vol. 12, no. 1, pp. 350–359, Mar. 2018.
[50] M. Bahrami, M. Vakilian, H. Farzin, and M. Lehtonen, "A stochastic framework for optimal island formation during two-phase natural disasters," *IEEE Syst. J.*, early access, Mar. 2, 2021, doi: 10.1109/JSYST.2021.3058453.
[51] M. Bahrami, M. Vakilian, H. Farzin, and M. Lehtonen, "Multi-step island formation and repair dispatch reinforced by mutual assistance after natural disasters," *Int. J. Electr. Power Energy Syst.*, vol. 126, Mar. 2021, Art. no. 106572.
[52] M. E. Baran and F. F. Wu, "Network reconfiguration in distribution systems for loss reduction and load balancing," *IEEE Power Eng. Rev.*, vol. 9, no. 4, pp. 101–102, Apr. 1989.
[53] (2019). *Critical Loads*. [Online]. Available: https://drive.google.com/open?id=15AIg3yF8FnrPwQytbk9F6pvklMNfN83x
[54] J.-G. Elie and J.-C. Ruel, "Windthrow hazard modelling in boreal forests of black spruce and jack pine," *Can. J. Forest Res.*, vol. 35, no. 11, pp. 2655–2663, Nov. 2005.
[55] L. E. Frelich and E. J. Ostuno, "Estimating wind speeds of convective storms from tree damage," *E-J. Severe Storms Meteorol.*, vol. 7, no. 9, pp. 1–19, Dec. 2012.
[56] H. Farzin, M. Fotuhi-Firuzabad, and M. Moeini-Aghtaie, "A stochastic multi-objective framework for optimal scheduling of energy storage systems in microgrids," *IEEE Trans. Smart Grid*, vol. 8, no. 1, pp. 117–127, Jan. 2017.
[57] H. Farzin, M. Fotuhi-Firuzabad, and M. Moeini-Aghtaie, "Stochastic energy management of microgrids during unscheduled islanding period," *IEEE Trans. Ind. Informat.*, vol. 13, no. 3, pp. 1079–1087, Jun. 2017.
[58] N. Growe-Kuska, H. Heitsch, and W. Romisch, "Scenario reduction and scenario tree construction for power management problems," in *Proc. IEEE Bologna Power Tech Conf.*, vol. 3, 2003, pp. 1–7.
[59] IEEE PES AMPS DSAS Test Feeder Working Group. (2014). *123-Bus Feeder*. [Online]. Available: http://ewh.ieee.org/soc/pes/dsacom/testfeeders/feeder123.zip

MAHDI BAHRAMI received the B.Sc. degree in electrical engineering from the Amirkabir University of Technology, Tehran, Iran, in 2013, and the M.Sc. and Ph.D. degrees in electrical engineering from the Sharif University of Technology, Tehran, in 2015 and 2021, respectively. In 2020, he was a Visiting Ph.D. Student with Aalto University, Espoo, Finland. His research interests include distribution system operation and planning, smart grids, and power system reliability and resilience.

MEHDI VAKILIAN (Senior Member, IEEE) received the B.Sc. degree in electrical engineering and the M.Sc. degree in electric power engineering from the Sharif University of Technology in Tehran, in 1978 and 1986, respectively, and the Ph.D. degree in electric power engineering from the Rensselaer Polytechnic Institute, Troy, NY, USA, in 1993. He worked with Iran Generation and Transmission Company (Tavanir), from 1981 to 1983, and then with the Iranian Ministry of Energy, from 1984 to 1985. Since 1986, he has been as a Faculty Member of the Department of Electrical Engineering, Sharif University of Technology. From 2001 to 2003 and from 2014 to 2018, he was the Chairperson of the Department. From 2003 to 2004 and in part of 2007, and from July 2018 to July 2019, he was on leave of study from the School of Electrical Engineering and Telecommunication, The University of New South Wales, Sydney. His research interests include transient modeling of power system equipment specially power transformers, optimum design of high voltage equipment insulation, monitoring and protection of power system equipment and their insulations specially with partial discharge measurement, power system transients, and distribution system studies, including its resiliency.

HOSSEIN FARZIN received the B.Sc. and Ph.D. degrees in electrical engineering from the Sharif University of Technology, Tehran, Iran, in 2011 and 2016, respectively. He was a Postdoctoral Researcher with the Sharif University of Technology, from 2016 to 2017. He is currently an Assistant Professor with the Electrical Engineering Department, Shahid Chamran University of Ahvaz, Ahvaz, Iran. His research interests include microgrids design and optimization, integration of distributed energy resources and electric vehicles in smart grid, and power system reliability and resilience. He ranked second in Iran's nationwide universities entrance exam, in 2007. He was a recipient of Iran's National Elites Foundation Scholarship for young assistant professors, in 2018. He serves as an Editor for *Scientia Iranica*.

MATTI LEHTONEN received the master's and Licentiate degrees in electrical engineering from the Helsinki University of Technology, in 1984 and 1989, respectively, and the Doctor of Technology degree from the Tampere University of Technology, in 1992. From 1987 to 2003, he was with VTT Energy, Espoo, Finland. Since 1999, he has been a Professor with the Helsinki University of Technology (now Aalto University), where he is currently the Head of the Power Systems and High Voltage Engineering. His research interests include power system planning and asset management, power system protection, including earth fault problems, harmonic related issues, and applications of information technology in distribution systems.